The Journal of CPRI,
Vol. 13, No. 1, March 2017 pp. 163-170

Generation and characterisation of nano iron oxide by wire explosion process: a thermodynamic approach

Prem Ranjan*, Yusuke Nakayama**, Santhosh Kumar L ***, Jayaganthan R****,
Suematsu H** and Sarathi R *,

Iron oxide (Fe_2O_3) nanoparticles were generated in a single step by wire explosion process (WEP). The influence of energy deposited to the exploding conductor and the ambient pressure on phase, size and shape of the particle were analysed. Oxygen is used as medium during wire explosion process to obtain iron oxide. The characteristics of the particles were analysed through WAXD and TEM. The thermodynamic aspects of nanoparticle formation by wire explosion process are detailed.

Keywords: *Nanoparticle; Wire Explosion; Iron Oxide; Born-Haber cycle; Nucleation rate*

1.0 INTRODUCTION

Synthesis of nanoparticles with controlled morphology, size and phase composition is of great interest due to its different physical and chemical properties compared to bulk material. Iron oxide nanoparticles are widely investigated due to its application in biomedicals [1] such as targeted drug delivery, tissue repair, Magnetic Resonance Imaging (MRI); waste water treatment [2] as nanoadsorbents and photocatalysts. Physical properties of nanoparticles can be varied by tailoringits size and shape. Magnetic property of iron oxide varies with different phases it form during synthesis under different process conditions.

Various methods used to synthesize iron oxide particles are gas phase processes [3] for continuous production, ball milling [4], thermal decomposition [5], sol-gel method [6] etc. All these synthesis processes require costly precursors and equipment, multiple steps and long preparation time. Wire Explosion Process (WEP) is one step method to produce nanoparticles of metals; metallic oxide, nitride, carbide etc. [7-10]. Here, high magnitude of current is flown through a metallic conducting wire in oxygen ambience to produce metallic oxide nanoparticles. Size of nanoparticles is controlled with ambient pressure and amount of deposited energy. The study of thermodynamic parameters on particle formation and its size is scarce in the literature.

In the present study, iron oxide is synthesized using WEP and characterised. X-ray diffraction (XRD) studies were conducted to detect the different phases of iron oxide formed. Morphology and size of the particles were analysed with transmission electron microscopy (TEM). Born-Haber cycle is adopted for calculating the lattice energy of the iron oxide. The prediction of dependence of lattice energy, nucleation rate and activation energy on different parameters was made through thermodynamic model.

2.0 EXPERIMENTAL STUDIES

Figure 1 shows experimental setup of WEP adopted in the present work. Capacitor, C is charged to

*Department of Electrical Engineering, IIT Madras, Chennai, 600036 India
**Extreme Energy-Density Research Institute, Nagaoka University of Technology, Nagaoka 940-2188, Japan
***Department of Aerospace Engineering, IIT Madras, Chennai, 600036, India
****Department of Engineering Design, IIT Madras, Chennai, 600036, India

the required voltage, V by DC voltage obtained after rectification of AC voltage by diode. Stored energy in the capacitor, $W= 0.5CV^2$ is deposited on iron wire after triggering the trigatron switch. Vapor of the exploded iron wire gets cooled, nucleates and reacts with ambience oxygen to form iron oxide nanoparticles. Figure 2 shows the typical voltage and current waveforms during the wire explosion measured with voltage probe (EP-50k, PEEC. A, Japan) and a current probe (Model No-101, Pearson Electronics, USA).

For the complete vaporization of iron wire, W should be greater than sublimation energy of iron, W_S. W_S of a material is calculated using [11]

$$W_S = C_S \times (T_m - T_r) + C_f \times (T_b - T_m) + h_m + h_v \quad (1)$$

Where, C_S are C_f are specific heat of the exploding metal in the solid and liquid state respectively, T_r, T_m, T_b are room, melting and boiling temperature respectively, h_m and h_v are latent heat of fusion and vaporization respectively.

For bulk Fe, calculated W_S is 7.81 kJ/g. Table 1 indicates the different parameters used in the present work. Here, ratio of W and W_S, K is varied for different values along with different P. In this work, XRD was performed by D8 Discover, Bruker diffractometer using Cu-Kα radiation of wavelength 1.5425Å at a scan rate of 9º/minute. PANalytical X'pert High score plussoftware was used for Rietveld refinement. TEM micrographs were captured by Philips CM12.

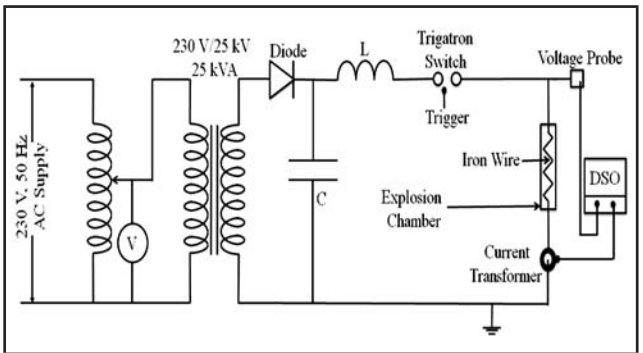

FIG. 1. EXPERIMENTAL SETUP OF WIRE EXPLOSION PROCESS

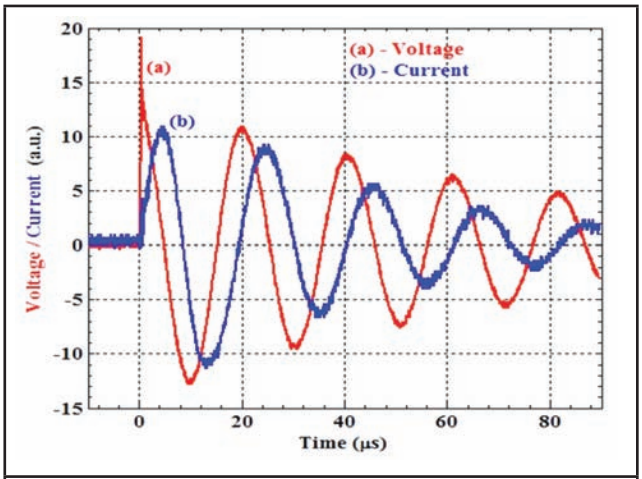

FIG. 2. TYPICAL VOLTAGE AND CURRENT WAVEFORMS MEASURED DURING WIRE EXPLOSION PROCESS

TABLE 1 WIRE EXPLOSION PROCESS EXPERIMENTAL PARAMETERS	
Capacitance, C	3 μF
Length of Fe wire	100 mm
Wire diameter (mm)	0.3, 0.1
Charging voltage (kV)	15, 21, 28
Oxygen pressure (kPa)	20, 100, 180

3.0 RESULTS AND DISCUSSIONS

3.1 XRD Studies

Figure 3 shows the XRD pattern of iron oxide produced for K=1 and different P. Pattern matches with JCPDS Card No. 033-0664 (Hematite or α-Fe_2O_3), JCPDS Card No. 039-1346 (Maghemite or γ-Fe_2O_3) and JCPDS Card No. 019-0629 (Magnetite or Fe_3O_4). It is very difficult to differentiate between XRD peaks of γ-Fe_2O_3 and Fe_3O_4 as they have same crystal lattice parameters. For K = 1, content of α-Fe_2O_3 decreases with reduction in P as evident from Figure 3. XRD pattern of iron oxide for different K, P are shown in Figure 4. For P=180 kPa, content of α-Fe_2O_3 decreases with increase in K. For K =3 also same trend follows as that for K = 1 with varying pressure. For P= 20 kPa, content of α-Fe_2O_3 decreases with increase in K from 3 to 10. So, for low P and high K, it is possible to minimise the content of α-Fe_2O_3 as evident from Figure 4 for P=20 kPa and K= 10 and 18. Full

oxidation of Iron is achieved in all cases as there is no peak corresponding to Iron in the XRD pattern.

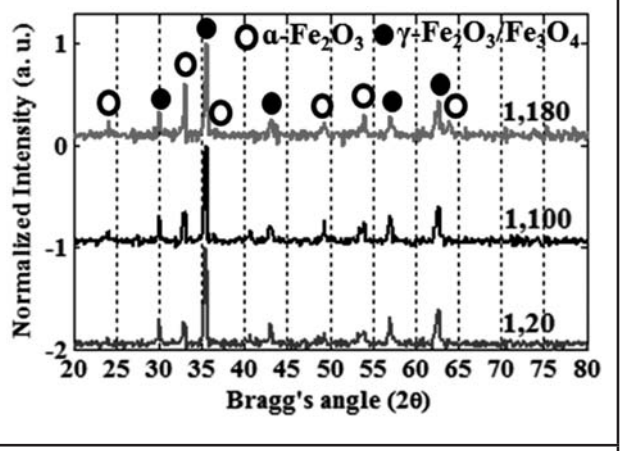

FIG. 3. XRD PATTERN OF IRON OXIDE PRODUCED BY WEP IN DIFFERENT O_2PRESSURE AT K = 1

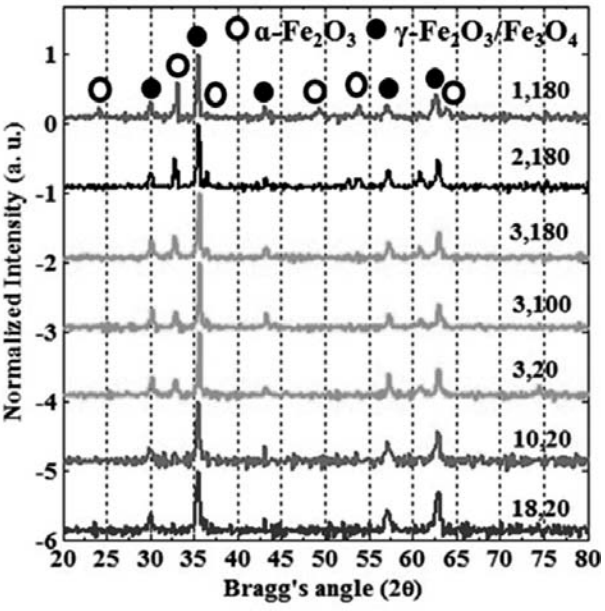

FIG. 4. XRD PATTERN OF IRON OXIDE PRODUCED BY WEP AT DIFFERENT ENERGY RATIO AND OXYGEN PRESSURE (K,P)

3.2 TEM Studies

Figure 5 shows the TEM images of Iron Oxide nanoparticles obtained by WEP. The synthesized particles have spherical and few have hexagonal shape. Heywood diameter [12] was used to determine the particle size diameters which vary from few nm to 300 nm. Particle size follows log-normal distribution [13].

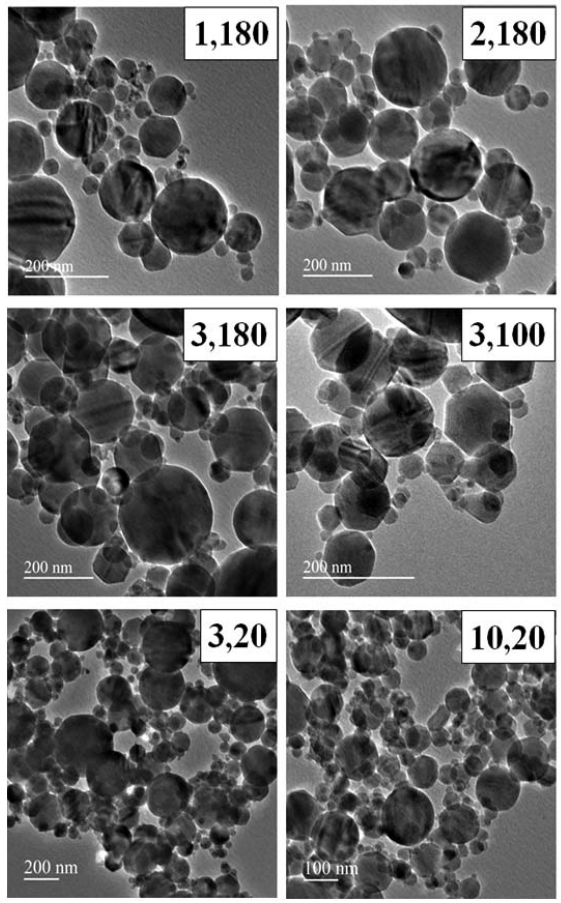

FIG. 5. TEM IMAGES OF IRON OXIDE PRODUCED BY WEP AT DIFFERENT ENERGY RATIO AND OXYGEN PRESSURE (K,P)

3.3 Particle size distribution studies

Figure 6 shows the Particle Size Distribution (PSD) of Iron Oxide obtained after exploding the iron wire in oxygen ambience at varying pressure with different deposited energy. For each case, 400-500 particle size was measured to determine the PSD. Table 2 shows the mean size and standard deviation of the Iron Oxide nanoparticles produced by WEP. It can be noted that mean particle size decreases with increasing K and/or decreasing ambient oxygen pressure. Least mean size of the particles is 38 nm for the parameters used in this work.

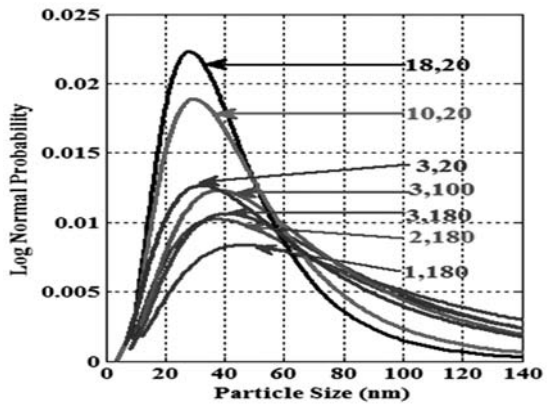

FIG 6. PARTICLE SIZE DISTRIBUTION OF IRON OXIDE PRODUCED BY WEP AT DIFFERENT ENERGY RATIO AND OXYGEN PRESSURE (K,P)

TABLE 2
VARIATION IN MEAN DIAMETER AND STANDARD DEVIATION OF FE_2O_3 NANOPARTICLES

Sample(K,P)	Mean Size (nm)	Standard deviation (nm)
1,180	83.50	2.14
2,180	68.06	2.16
3,180	68.03	2.03
3,100	60.25	1.97
3,20	56.07	2.09
10,20	42.42	1.81
18,20	38.00	1.76

3.4 Formation of enthalpy and lattice energy

In the present model, it is assumed that in WEP, reaction takes place in vapor state. Standard formation of enthalpy of iron oxide when the constituent Fe and molecular O_2 are in their standard state of solid and gas is given by

$$2\,Fe\,(s) + 1.5\,O_2(g) \rightarrow Fe_2O_3(s) \quad ...(2)$$

$$: \Delta H^0_{f,Fe_2O_3} = W_S = -826.2 \pm 1.3\ kJ/mol$$

We have considered the formation of α-Fe_2O_3 in our model. For other iron oxides, one can calculate on the similar line. To get the lattice energy (LE) of Fe_2O_3, we consider the ionic state reaction for the formation of Fe_2O_3 as

$$2\,Fe^{3+}(g) + 3\,O^{2-}(g) \rightarrow Fe_2O_3(s) \quad ...(3)$$

$$: \Delta H_{f,Fe_2O_3} = LE = -14606.54737\ kJ/mol$$

Lattice energy is calculated using Born Haber cycle as shown in figure7 given by

$$LE = 2\,(W_s)_{Fe} + \Delta H^0_{f,Fe_2O_3} + 2\sum_{i=1}^{3}(IE_i)_{Fe} + 1.5\,(BDE)_{O_2} + 3\sum_{j=1}^{2}(EA_j)_O \quad ...(4)$$

Where, IE_i is the ionization energy of i^{th} oxidation state of Fe, BDE is the bond dissociation energy of molecular oxygen and EA_j is the electron affinity of j^{th} reduction state of atomic oxygen. All the values needed to calculate LE and stepwise reaction enthalpy of Born-Haber cycle is given in Table 3.

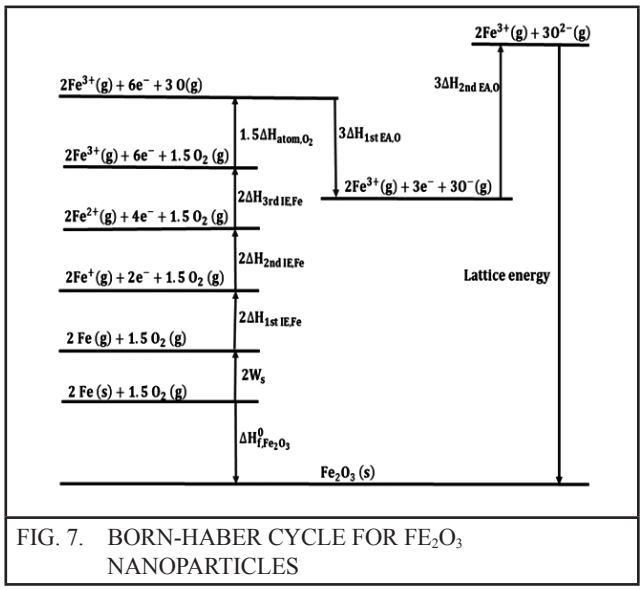

FIG. 7. BORN-HABER CYCLE FOR FE_2O_3 NANOPARTICLES

TABLE 3
INDIVIDUAL STEP REACTION ENTHALPIES OF BORN-HABER CYCLE FOR FE_2O_3.

Parameter	Magnitude (kJ/mol)
W_s	435.960414
$\Delta H_{1st\ IE,Fe}$	762.463064
$\Delta H_{2nd\ IE,Fe}$	1561.870235
$\Delta H_{3rd\ IE,Fe}$	2957.45822
BDE or $\Delta H_{atom,O_2}$	249.229
$\Delta H_{1st\ EA,O}$	-141.0
$\Delta H_{2nd\ EA,O}$	798.0
LE	14606.54737
$\Delta H^0_{f,bulk}$ or $\Delta H^0_{f,Fe_2O_3}$	-826.2

3.5 Size Dependent Lattice Energy (Sdle) Of Fe_2o_3 Nanoparticles

Nanda's SDCE model [14,15] is modified to determine the size dependent lattice energy (SDLE) of the Fe_2O_3 nanoparticle (a_{v,d,Fe_2O}). Multiple of atomic fractions of Fe and O with their corresponding SDCE ($a_{v,d}$) are added to give a_{v,d,Fe_2O_3} as shown

$$a_{v,d,Fe_2O_3\ np} = \left(\frac{2}{5}\right) a_{v,d,Fe} + \left(\frac{3}{5}\right) a_{v,d,O} \quad ...(5)$$

$$a_{v,d,Fe_2O_3} = \left(\frac{2}{5}\right) a_v \left[1 - \frac{N_{s,}}{N}\left(1 - \sqrt{\frac{Z_{s,Fe}}{Z_{b,Fe}}}\right)\right] + \left(\frac{3}{5}\right) a_v \left[1 - \frac{N_{s,O}}{N}\left(1 - \sqrt{\frac{Z_{s,O}}{Z_{b,O}}}\right)\right] \quad ...(6)$$

Here, a_v is the bulk lattice energy of Fe_2O_3 calculated from eqn. 3 and 4, N is the total number of atoms in a spherical nanoprticle, N_s is the number of its surface atoms and Z_s and Z_b respectively are the surface and coordination numbers of the nanoparticle. For a spherical nanoparticle of diameter d containing individual atoms of radius r_a, $N_s/ N = 8\ r_a/d$.

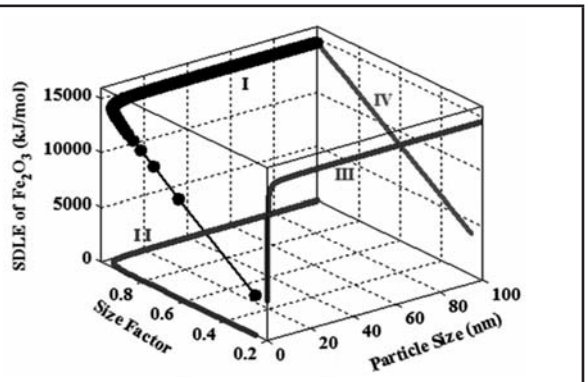

FIG. 8. SDLE OF FE_2O_3 NANOPARTICLES

Hematite has a rhombohedral structure wherein Fe is occupying octahedral site having a coordination number 6 and O is having a coordination number 4. Hence, for Fe and O in Fe_2O_3, $Z_{s,Fe}/ Z_{b,Fe} = 5/6$ and $Z_{s,O}/ Z_{b,O} = 3/4$.

After simplification,

$$a_{v,d,Fe_2O_3} = a_v\ \varepsilon \quad ...(7)$$

Where, size factor

Where, size factor $\varepsilon = 1 - 0.26795\left(\frac{0.1394\ d_{Zn} + 0.3216\ d_O}{d_p}\right)$

Eqn. 7 is plotted as Figure 8 which shows that the SDLE of Fe_2O_3 decreases with decrease in size of nanoparticle.

3.6 Activation Energy for Formation of Fe_2O_3 Nuclei

When vapor phase starts to condense, the new phase nucleation happens when the embryos reaches critical diameter (r^*). Classical nucleation theory shows that bulk volume free energy (ΔG_v) and surface free energy (ΔG_s) are two components of Gibbs free energy (ΔG_v) to form spherical nucleus of radius r given by

$$\Delta G_{tot} = \frac{4\pi r^3 . \Delta\mu}{3v_{Fe_2O_3}} + 4\pi r^2 . \gamma_{Fe_2O_3} \quad ...(8)$$

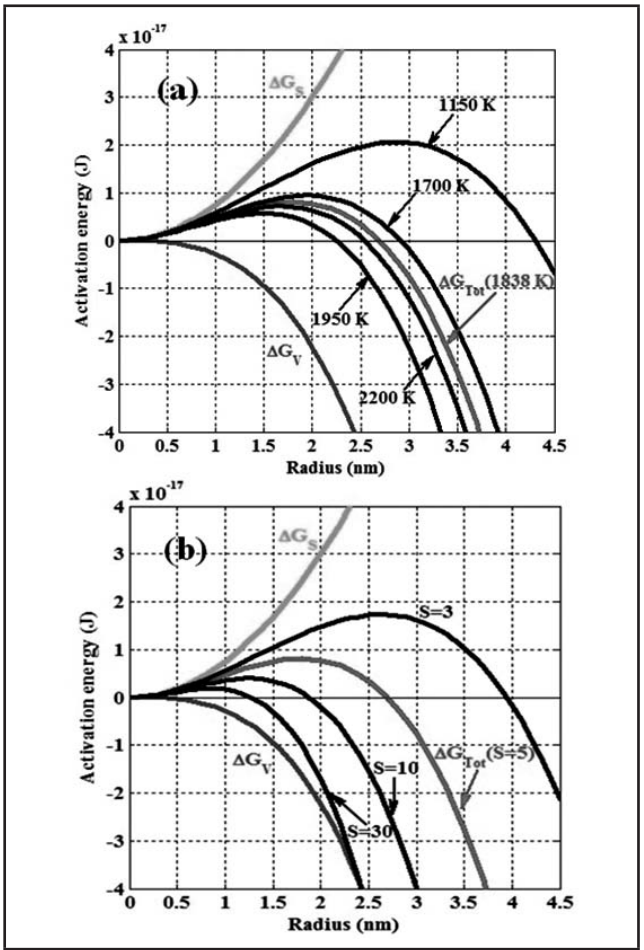

FIG. 9. ACTIVATION ENERGY OF NUCLEATION AT DIFFERENT (A) TEMPERATURE, (B) SATURATION RATIOS.

where, $\gamma_{Fe_2O_3}$ is the solid-vapor interfacial energy of Fe_2O_3 and $\Delta\mu$ is the chemical potential of Fe_2O_3 which is a function of temperature (T) and saturation ratio (S) and is given as, $\Delta\mu = -RT.\ln(S)$. Eqn. 8 is plotted as Figure 9 keeping S constant and T varying for one case and vice versa for another. It is evident from figure 8 that with increase in T or S, activation energy decreases causing decrement in activation barrier, consequently nucleation rate increases, yielding lower sized particles.

The critical size (r_c) and its corresponding activation energy ($\Delta G^*(r_c)$) of the nucleus is given as

$$r_c = -\frac{2\gamma_{Fe_2O_3}}{\Delta\mu} = \frac{2\ Fe_2O_3}{\ln(S)} \quad ...(9)$$

$$\Delta G^*(r_c) = \frac{16\pi\gamma^3_{Fe_2O_3}}{3(\Delta\mu)^2} = \frac{4\pi r_c^2\gamma_{Fe_2O_3}}{3} \quad ...(10)$$

From eqn. 9 and 10, we can say that with increase in supersaturation, there is decrease in critical radius and the activation energy.

3.7 Nucleation rate of Fe_2O_3 nanoparticles

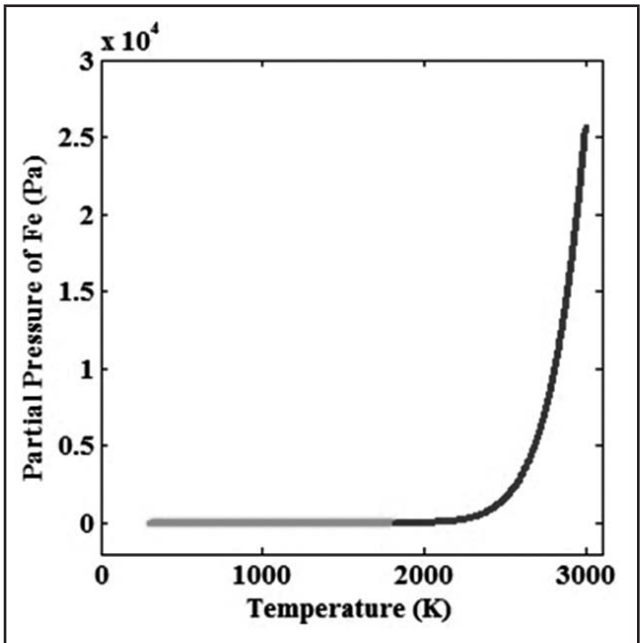

FIG.10. PARTIAL PRESSURE OF IRON VAPOR AS A FUNCTION OF TEMPERATURE

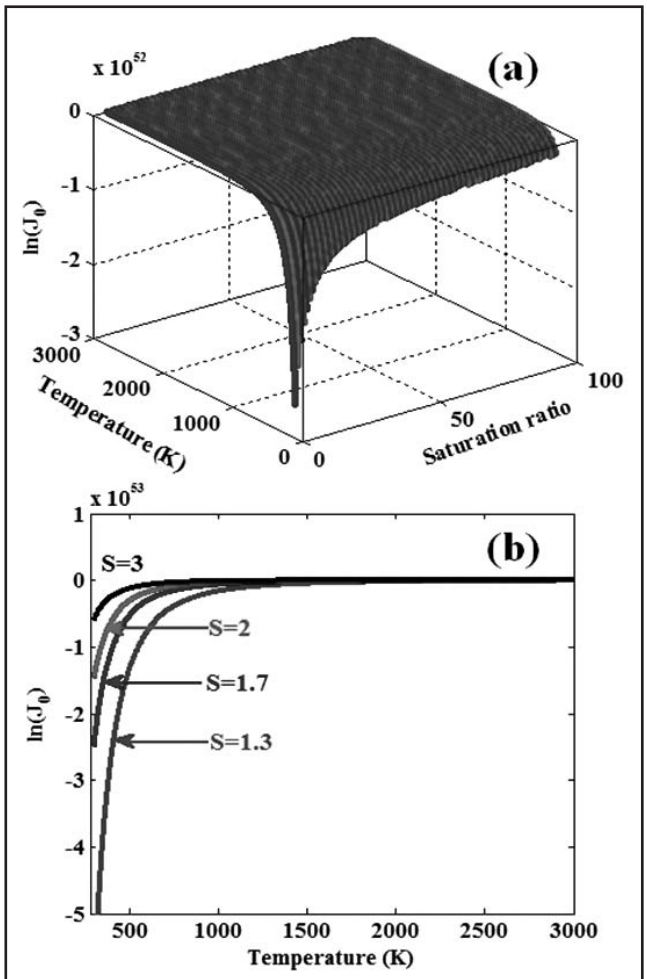

FIG. 11. NUCLEATION RATE OF FE_2O_3 AS A FUNCTION OF (A) SATURATION RATIO AND TEMPERATURE (B) TEMPERATURE AT DIFFERENT SATURATION RATIOS

In the present work, we assume reaction takes place in vapor state and Fe_2O_3 vapor behaves as an ideal gas. According to classical nucleation expression, nucleation rate, J_o can be expressed as

$$J_0 = \left(\frac{P_{Fe_2O_3}}{kT}\right)^2 . \sqrt{\frac{2\sigma_{Fe_2O_3}}{\pi M}} . \exp\left\{-\frac{16\pi\sigma^3 v^2_{Fe_2O_3}}{3(kT)^3.(\ln S)^2}\right\} ..(11)$$

where, M is the molecular weight of Fe_2O_3, k is the Boltzmann constant, $\sigma_{Fe_2O_3}$ is surface tension of molten Fe_2O_3, $P_{Fe_2O_3}$ is total pressure of the product Fe_2O_3 gas, $v_{Fe_2O_3}$ is the molar volume of Fe_2O_3 at its melting temperature and 1 atm. Here, $P_{Fe_2O_3}$ is the sum of partial pressures of Fe vapor ($P_{Fe_2O_3}$) and oxygen (P_{O_2}) i.e. $P_{Fe_2O_3} = P_{Fe} + P_{O_2}$ where,

$$\log_{10}(P_{Fe})_{Solid} = 16.89 - \frac{}{T} - 2.14\log(T)$$
:900 K≤T≤mp

$$\log_{10}(P_{Fe})_{Liquid} = 13.27 - \frac{19710}{T} - 1.27\log(T)$$
:mp≤T≤3000 K

Now substituting,

$$J_0 = K_1 . \exp\left\{-\frac{K_2}{(kT.\ln S)^2}\right\} \quad (12)$$

Where, $K_1 = \left(\frac{P_{Fe}+P_{O_2}}{kT}\right)^2 . \sqrt{\frac{2\sigma_{Fe_2O_3}}{\pi M}} . v_{Fe_2O_3}$ and

$$K_2 = \frac{16\pi\sigma^3 v_{Fe_2O_3}^2}{3kT}$$

Plot of $P_{Fe_2O_3}$ as a function of T is shown in Figure 10. $P_{Fe_2O_3}$ increases rapidly after 2000 K showing flaw in ideal behavior of mixture of oxygen gas and iron vapor. Figure 11 shows the variation of computed nucleation rate of Fe_2O_3 as a function of S and T. It is evident from Figure 11 (a), nucleation rate is high for any saturation ratio at higher temperatures, consequently giving lower sized particles. It can be concluded from Figure 11 (b) that for any temperature, nucleation rate increases with increase in saturation ratio.

4.0 CONCLUSIONS

Iron Oxide nanoparticles were produced by WEP by exploding Iron wire in oxygen ambience confirmed with XRD studies. Particle size and shape were analysed with TEM micrographs. Particles are hexagonal and spherical in shape and size of particles varies from few nm to submicron size. The particles formed by WEP follows Log-normal distribution and the mean size of the particle obtained by WEP is 38 nm. The results of the study confirms that with higher K and low oxygen ambience pressure, content of α-Fe_2O_3 nanoparticles can be minimized. Bulk and size dependent lattice energy is calculated. With increase in energy ratio K, temperature increases,leading to higher nucleation rate resulting in lower sized nanoparticles. Based on Gibbs free energy calculations, one can determine the critical nucleus radius and its activation free energy by varying the saturation ratio and vapor temperature.

REFERENCES

[1] A. K. Gupta and M. Gupta, "Synthesis and surface engineering of iron oxide nanoparticles for biomedical applications," Biomaterials, Vol. 26, No. 18, pp. 3995–4021, 2005.

[2] P. Xu *et al*., "Use of iron oxide nanomaterials in wastewater treatment: A review," Sci. Total Environ., Vol. 424, pp. 1–10, 2012.

[3] F. E. Kruis, H. Fissan, and A. Peled, "Synthesis of nanoparticles in the gas phase for electronic, optical and magnetic applications—a review," J. Aerosol Sci., Vol. 29, No. 5–6, pp. 511–535, 1998.

[4] L. L. Wang and J. Sen Jiang, "Preparation of α-Fe2O3 nanoparticles by high-energy ball milling," Phys. B Condens. Matter, Vol. 390, No. 1–2, pp. 23–27, 2007.

[5] K. Woo et al., "Easy Synthesis and Magnetic Properties of Iron Oxide Nanoparticles," Chem. Mater., No. 8, pp. 2814–2818, 2004.

[6] J. Xu et al., "Preparation and magnetic properties of magnetite nanoparticles by sol-gel method," J. Magn. Magn. Mater., Vol. 309, No. 2, pp. 307–311, 2007.

[7] W. Jiang and K. Yatsui, "Pulsed wire discharge for nanosize powder synthesis," IEEE Trans. Plasma Sci., Vol. 26, No. 5, pp. 1498–1501, 1998.

[8] R. Sarathi, T. K. Sindhu, S. R. Chakravarthy, A. Sharma, and K. V. Nagesh, "Generation and characterization of nano-tungsten particles formed by wire explosion process," J. Alloys Compd., Vol. 475, No. 1–2, pp. 658–663, 2009.

[9] Y. a. Kotov, "Electric explosion of wires as a method for preparation of nanopowders," J. Nanoparticle Res., Vol. 5, No. 5–6, pp. 539–550, 2003.

[10] H. Suematsu *et al.*, "Repetitive pulsed wire discharge for applications to material science," Conf. Rec. Twenty-Fifth Int. Power Modul. Symp. 2002 2002 High-Voltage Work., pp. 138–141, 2002.

[11] S. I. Tkachenko, V. S. Vorob'ev, and S. P. Malyshenko, "The nucleation mechanism of wire explosion," J. Phys. D. Appl. Phys., Vol. 37, No. 3, pp. 495–500, 2004.

[12] Yasuo Arai, Chemistry of Powder Production, 1 st ed., Chapman & Hall, London, 1996.

[13] Bernhardt C, Particle Size Analysis: Classification and Sedimentation Methods, 1st ed., Chapman & Hall, London, 1994.

[14] K. K. Nanda, S. N. Sahu, and S. N. Behera, "Liquid-drop model for the size-dependent melting of low-dimensional systems," Phys. Rev. A., No. 66, pp. 1–8, 2002.

[15] RS. C. Vanithakumari and K. K. Nanda, "Phenomenological Predictions of Cohesive Energy and Structural Transition of Nanoparticles," J. Phys. Chem. B., No. 1102, pp. 1033–1037, 2006.